OPEN ACCESS

Original research

Histone lactylation-driven feedback loop modulates cholesterol-linked immunosuppression in pancreatic cancer

Jing Yang ,[1,2,3,4,5] Xiaoning Yu ,[1,2,3,4,5] Mingming Xiao ,[1,2,3,4,5] He Xu ,[6] Zhen Tan ,[7] Yubin Lei ,[8] Yanmei Guo ,[9] Wei Wang ,[1,2,3,4,5] Jin Xu ,[1,2,3,4,5] Si Shi ,[1,2,3,4,5] Xianjun Yu [1,2,3,4,5]

► Additional supplemental material is published online only. To view, please visit the journal online (https://doi.org/10.1136/gutjnl-2024-334361).

For numbered affiliations see end of article.

Correspondence to
Professor Xianjun Yu; yuxianjun@fudanpci.org and Dr Si Shi; shisi@fudanpci.org

JY, XY and MX contributed equally.

JY, XY and MX are joint first authors.
SS and XY are joint senior authors.

Received 14 November 2024
Accepted 22 May 2025

Check for updates

© Author(s) (or their employer(s)) 2025. Re-use permitted under CC BY-NC. No commercial re-use. See rights and permissions. Published by BMJ Group.

To cite: Yang J, Yu X, Xiao M, *et al*. *Gut* Epub ahead of print: [*please include* Day Month Year]. doi:10.1136/gutjnl-2024-334361

ABSTRACT

Background Pancreatic cancer exhibits limited clinical responses to immunotherapy, highlighting the need for new strategies to counteract its immunosuppressive microenvironment. Although metabolic reprogramming and epigenetic changes contribute to malignancy, the impact of lactate-driven histone lactylation on the tumour microenvironment (TME) has not been fully explored.

Objective This study aims to investigate the role of histone lactylation in pancreatic cancer, focusing on its effects on cholesterol metabolism and antitumour immunity.

Designs Global lactylome profiling was conducted to identify novel epigenetic mechanisms driven by lactate-induced histone lactylation. Mechanisms were investigated via RNA sequencing, CUT&Tag, immunoprecipitation-mass spectrometry and GST-pull down. Mass cytometry by time-of-flight, *in vitro* co-culture system, orthotopic pancreatic cancer models and flow cytometry were used to explore Acetyl-CoA acetyltransferase (ACAT2) functions. A proteolysis-targeting chimaera (PROTAC) was developed to degrade ACAT2.

Results Global lactylome profiling revealed that lactate-driven histone lactylation, particularly H3K18la, promotes the transcriptional activation of ACAT2. ACAT2 acetylates mitochondrial carrier homolog 2 (MTCH2), stabilising it and disrupting oxidative phosphorylation, which increases lactate production and fuels a positive feedback loop in pancreatic cancer. This loop facilitates the delivery of cholesterol via small extracellular vesicles (sEVs), polarising tumour-associated macrophages toward an immunosuppressive M2 phenotype. Additionally, the PROTAC targeting ACAT2 enhanced the efficacy of immune checkpoint blockade therapy *in vivo*.

Conclusions Our findings highlight the critical role of the H3K18la/ACAT2/sEV-cholesterol axis in TME reprogramming. Targeting this pathway may improve anti-PD-1 therapy response in pancreatic cancer, providing a novel therapeutic strategy by linking histone lactylation, cholesterol metabolic reprogramming and immune modulation.

WHAT IS ALREADY KNOWN ON THIS TOPIC

⇒ Lactate-derived lactylation of histone lysine residues functions as an epigenetic modification that directly enhances gene transcription from chromatin, highlighting its therapeutic potential in cancer treatment.
⇒ Cholesterol induces immunosuppression by activating immune cells such as $CD8^+$ T cells, but its function remains controversial.

WHAT THIS STUDY ADDS

⇒ Lactate-driven histone lactylation regulates ACAT2 transcription in pancreatic cancer.
⇒ ACAT2-mediated MTCH2 K100 acetylation disrupts oxidative phosphorylation and boosts lactate production in pancreatic cancer.
⇒ ACAT2 facilitates cholesterol transfer via small extracellular vesicles, thereby polarises M2-like tumour-associated macrophages and promotes immune desert formation.
⇒ Degradation of ACAT2 with a proteolysis-targeting chimaera sensitises pancreatic cancer cells to immune checkpoint blockade (ICB) therapy.

HOW THIS STUDY MIGHT AFFECT RESEARCH, PRACTICE OR POLICY

⇒ Our results open a new window on the role of ACAT2 in regulating metabolic reprogramming and antitumour immunity and propose a more effective strategy for tumour immunotherapy by combining ACAT2 degradation with ICB.

INTRODUCTION

With an upsetting 5-year overall survival (OS) rate of approximately 13%, pancreatic cancer is acknowledged as one of the most aggressive cancers.[1] A staggering 80% of patients experience disease recurrence despite undergoing surgical resection, underscoring the cancer's tendency for rapid relapse.[2] Moreover, standard treatments such as chemotherapy combined with radiotherapy often result in only transient partial remissions or stable disease in newly diagnosed patients.[3] A major obstacle that leads to the unfavourable outcome for pancreatic cancer patients is the scarcity of efficacious treatment targets.[4 5] For instance, while immunotherapy, particularly immune checkpoint inhibitors, has shown promise in various solid tumours, nearly all clinical trials have reported

minimal benefit from mono-immunotherapy in pancreatic cancer patients.[6 7] Consequently, clarifying the basic processes behind immune evasion in pancreatic cancer and identifying strategies to enhance responses to immunotherapy are crucial for improving long-term outcomes.

Recent studies have identified various histone acylations derived from cellular metabolites, including propionylation, butyrylation and lactylation, among others.[8] A new type of post-translational modification (PTM), histone lactylation, was discovered 5 years ago, representing a new epigenetic mode that drives gene transcription.[9] Lactylation, primarily facilitated by lactate, a byproduct of cellular metabolism, transforms our perception of lactate from a metabolic waste to a crucial regulator of gene expression and protein functionality.[9 10] Various PTMs play pivotal roles in tumour progression, including malignant cell proliferation, immune cell activation and metabolic reprogramming, underscoring their therapeutic potential in cancers.[11–14] However, the specific roles of histone lactylation in mediating tumour progression and immune evasion in pancreatic cancer remain poorly understood.

In this study, we demonstrate that H3K18la is generally elevated in pancreatic cancer, with specific enrichment at the promoter of Acetyl-CoA acetyltransferase 2 (ACAT2). As an acetyltransferase, ACAT2 forms a positive feedback loop with lactate and H3K18la, exacerbating lactate accumulation and tumour progression. Notably, the overexpression of ACAT2, driven by this feedback loop, enhances immunosuppression through the promotion of M2 macrophage polarisation. Additionally, ACAT2 facilitates cholesterol biosynthesis, which further supports M2 polarisation. We also employed a proteolysis-targeting chimaera (PROTAC) to degrade ACAT2 *in vivo*, proposing an effective strategy for tumour immunotherapy by combining ACAT2 degradation with immune checkpoint blockade (ICB) in pancreatic cancer.

MATERIALS AND METHODS

Additional materials and methods are included in the online supplemental material.

RESULTS

H3K18la is the most prevalent histone modification with an unfavourable prognosis in pancreatic cancer

Given the shift from OXPHOS to elevated glycolysis,[15] we assessed lactate levels in pancreatic cancer. Colourimetric assays revealed higher lactate levels in pancreatic cancer tissues (online supplemental figure S1A and table S1). Proteome and lactylome analysis were conducted using paired tumour and normal tissues (figure 1A, online supplemental figure S1B–D), which identified a total of 7439 proteins and 4726 lactylation (Kla) sites distributed among 1895 proteins (online supplemental figure S1E–G). Notably, tumours exhibited a higher number of Kla sites compared with paired non-tumour counterparts (figure 1B). The overall abundance and variety of lactylation modifications were markedly increased in pancreatic cancer tissues (figure 1C,D).

It has been established that histone lactylation is essential for promoting gene transcription.[9 12] Our study identified 90 distinct Kla sites on various histones, with more histone Kla sites in tumour tissues (figure 1E,F). Additionally, we demonstrated a global increase in histone lactylation sites in pancreatic cancer (figure 1G). Supervised clustering of Kla sites also demonstrated significant differences in histone-related lactylation in tumour tissues (figure 1H), identifying 41 differentially expressed Kla sites, including the uniquely downregulated histone acetyltransferase KAT7 K322 site (T/N ratio 0.16) (figure 1I). Notably, H3K18la showed the most pronounced increase (figure 1I, online supplemental figure S1H,I). In the process of analysis, we normalised the proteomics data to exclude the potential influence of protein abundance on the lactylation level and finally identified the significant enrichment of H3K18la in tumour tissues (online supplemental figure S1J–L).

We observed significantly higher H3K18la in tumour tissues via immunofluorescence staining and western blot, which was associated with poorer prognosis and more advanced T stages (figure 1J–M, online supplemental figure S1M). The clinical characteristics of the patients in this cohort are presented in online supplemental table S2. Given that lactate serves as a precursor that can derive histone lactylation, we treated pancreatic cancer cells with varying concentrations of lactate and glycolysis inhibitors, including 2-deoxy-D-glucose (2-DG) and oxamate (online supplemental figure S1N,O). Lactate exposure increased intracellular lactate and H3K18la levels dose-dependently, while 2-DG and oxamate reduced both (figure 1N–P, online supplemental figure S1P–R). These findings indicate H3K18la as the most prevalent differentially enriched histone lactylation modification in pancreatic cancer and highlight its potential role in promoting pancreatic cancer progression.

Genome-wide analysis of the transcriptional consequences of H3K18la in pancreatic cancer

Histone lactylation has been shown to directly regulate gene transcription.[9 12] Hence, we conducted genome-wide CUT&Tag to identify genes potentially regulated by H3K18la. Significant enrichment of H3K18la peaks was observed in untreated PANC-1 and CFPAC-1 cells compared with those treated with oxamate for 24 hours (figure 2A). Promoter region H3K18la peaks (±3 kb) also decreased following oxamate treatment (figure 2B). KEGG analysis and gene ontology analysis of genes with H3K18la binding peaks in both PANC-1 and CFPAC-1 cells underscored the crucial roles of H3K18la in pancreatic cancer (figure 2C, online supplemental figure S2A).

Next, we performed RNA-seq to analyse transcriptional alterations after histone lactylation inhibition (figure 2D). Differentially expressed genes were visualised using volcano plots (online supplemental figure S2B). We integrated CUT&Tag with RNA-seq to pinpoint target genes activated by H3K18la, focusing on two candidate genes (figure 2E). We observed a notable decrease in ACAT2 expression in cells treated with oxamate, prompting further investigation into this gene (online supplemental figure S2C). Integrative Genomics Viewer analysis revealed enriched H3K18la at the ACAT2 promoter, with reduced signals at the transcription start site after oxamate treatment (figure 2F). ChIP analysis further confirmed diminished H3K18la levels at the ACAT2 promoter in oxamate-treated cells (figure 2G,H). Additionally, immunofluorescence staining showed higher ACAT2 expression in cancer tissues, positively correlating with H3K18la levels (figure 2I–K). Through FUSCC cohort analysis, we found that high ACAT2 correlated with poorer prognosis in pancreatic cancer (online supplemental figure S2D).

Histone deacetylase (HDAC) 1–3 serve as histone lysine delactylases, and acetyltransferase p300 acts as a putative histone Kla 'writer'.[9 16] Administration of the p300 inhibitor C646 reduced H3K18la and ACAT2, whereas trichostatin A (TSA), an HDAC inhibitor, had no effect on both of them (figure 2L,M, online supplemental figure S2E,F). These findings indicate that lactate accumulation is enough to activate ACAT2 expression through H3K18la. ChIP assays

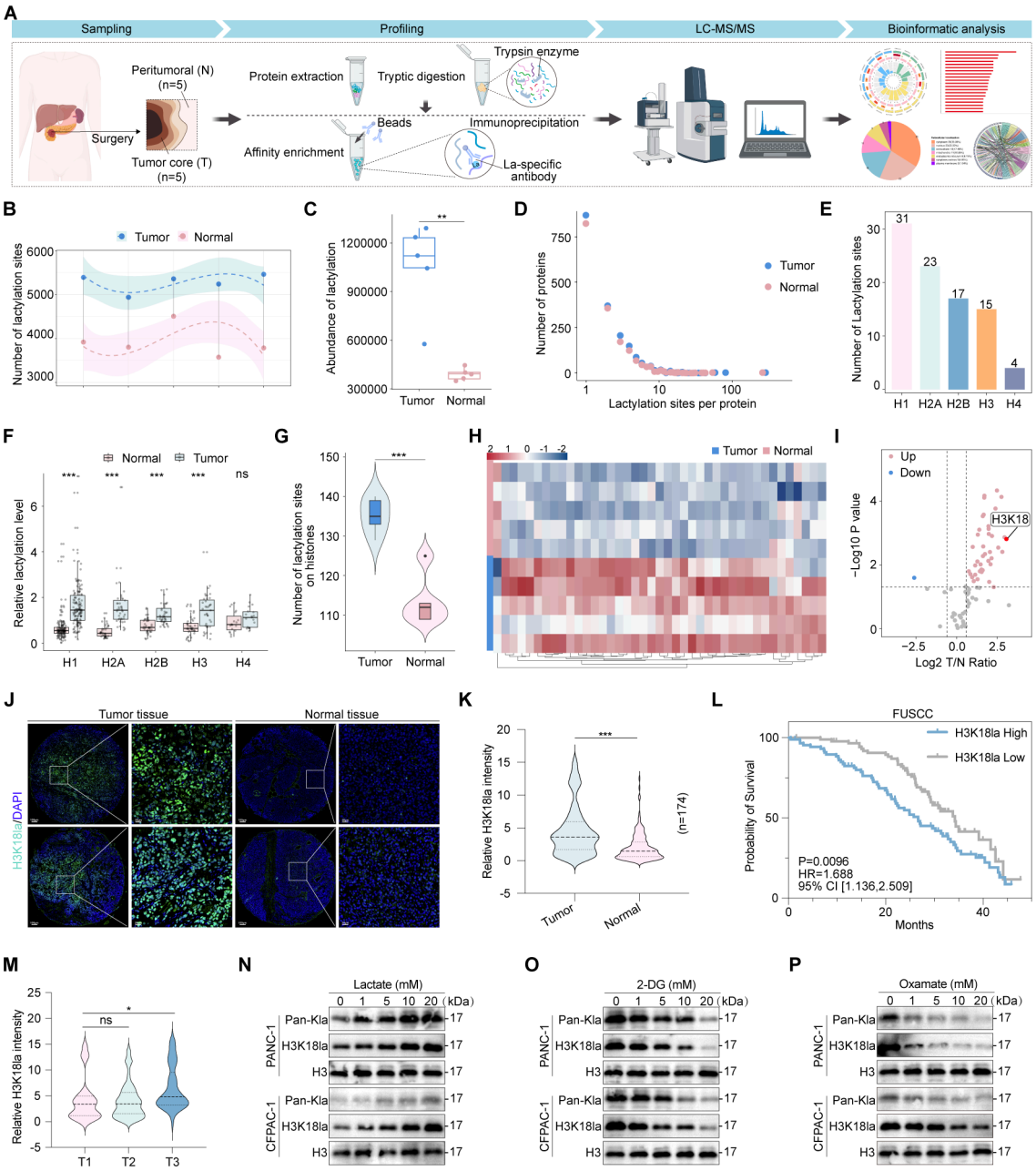

Figure 1 H3K18la is the most prevalent histone modification with an unfavourable prognosis in pancreatic cancer. (A) Schematic overview of the lysine lactylome and proteome analysis in pancreatic cancer (n=5) and paired normal tissues (n=5) using label-free quantification. (B) Overview of Kla identifications in pancreatic cancer (blue, n=5) and non-tumour (red, n=5) samples. Paired samples are connected by grey straight lines, and the shaded areas beneath the lasso curves represent the 95% CIs. (C) Quantitative analysis of the overall abundance of Kla in pancreatic samples (n=5 per group). Two-tailed paired t-test. (D) Number of Kla sites per protein in pancreatic cancer and paired normal tissues (n=5 per group). (E) Quantification of Kla sites on different histones in pancreatic samples (n=10). (F) Lactylation levels on specific histones are shown. Two-tailed unpaired t-test. (G) Violin plot showing the identified histone Kla sites between pancreatic cancer and adjacent normal tissues (n=5 per group). Two-tailed paired t test. (H, I) Heatmap (H) and volcano plot (I) analysis showing Kla sites altered on histones in pancreatic cancer (n=5 per group). (J, K) Representative images (J) and quantification (K) of H3K18la levels visualised by immunofluorescence staining in tumour and normal tissues (n=174). Scale bar: left panel, 100 µm; right panel, 20 µm. Two-tailed paired t-test. (L) Kaplan-Meier analysis of the overall survival of patients with pancreatic cancer from FUSCC based on H3K18la levels (n=174). Log rank test. (M) H3K18la levels in pancreatic cancer patients at AJCC stages T1 to T3. Two-tailed unpaired t-test. (N–P) Western blot analysis of H3K18la levels measured from PANC-1 and CFPAC-1 cells cultured in different concentrations (0 mM, 1 mM, 5 mM, 10 mM, 20 mM) of lactate (N), 2-DG (O) and oxamate (P) for 24 hours. Data are represented as the mean±SD. *p<0.05; **p<0.01; ***p<0.001; ns, not significant. 2-DG, 2-deoxy-D-glucose; AJCC, the american joint committee on cancer.

demonstrated that EP300 knockdown decreased the enrichment of H3K18la at the ACAT2 promoter (figure 2N–P, online supplemental figure S2G), supporting the role of H3K18la in ACAT2 transcriptional regulation. We next generated ACAT2 knockout cell lines using CRISPR-Cas9 and re-expressed CRISPR-resistant ACAT2 (online supplemental figure S2H). Colony formation and CCK-8 assays confirmed the role of ACAT2 in prompting the growth of

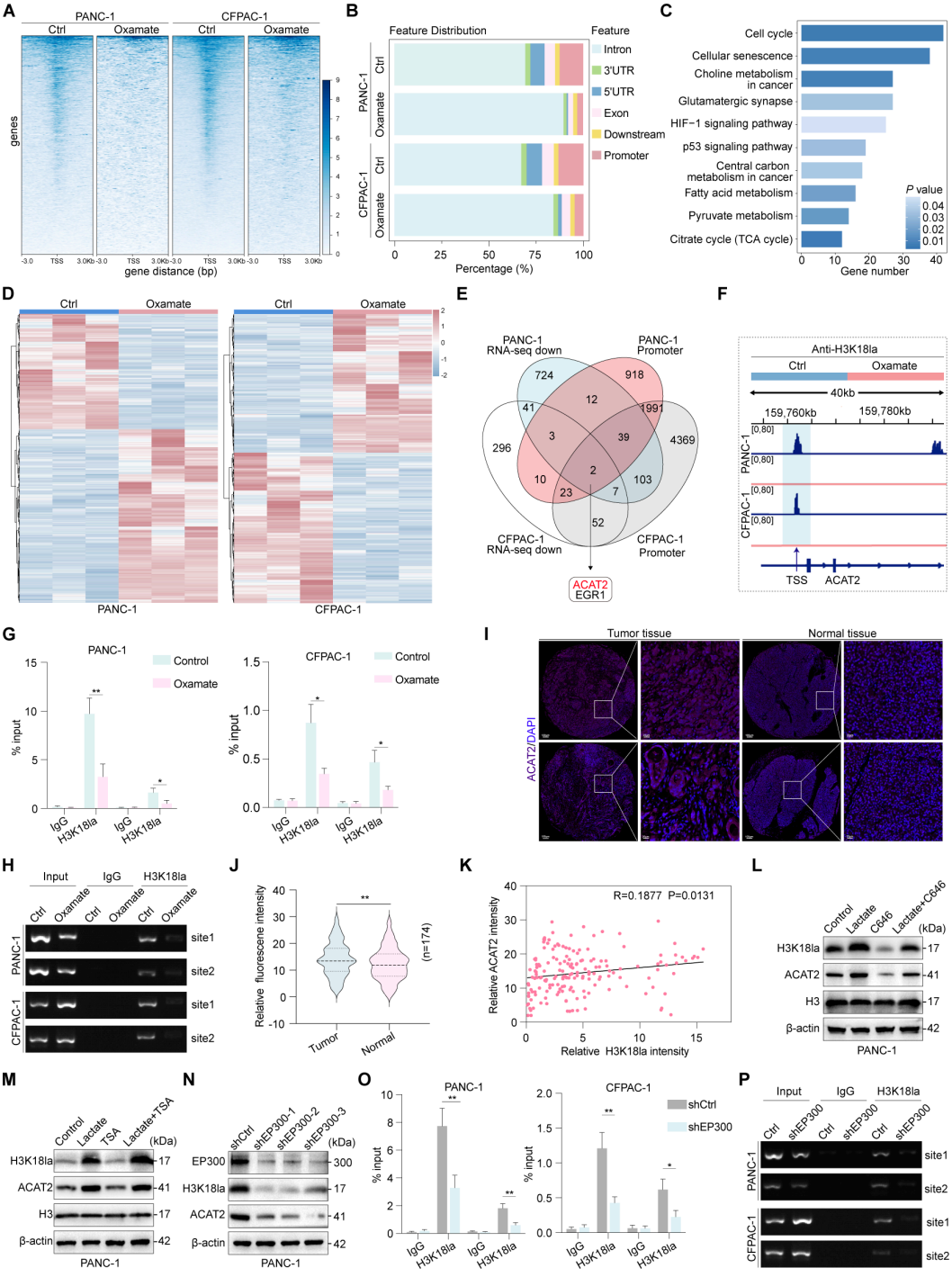

Figure 2 Genome-wide analysis of the transcriptional consequences of H3K18la in pancreatic cancer. (A) The binding density of H3K18la visualised using deepTools, showing the CUT&Tag tag counts at different H3K18la binding peaks in PDAC cell lines treated with or without 20 mM oxamate for 24 hours. (B) Stacked bar plots showing genomic annotation of H3K18la binding regions in different groups. (C) Bar plot showing the KEGG analysis of the candidate target genes with H3K18la binding peaks in both PANC-1 and CFPAC-1 cells. (D) Heatmap indicating the expression of DEGs involved in different groups via RNA-seq. (E) Venn Diagram of CUT&Tag and RNA-seq between PANC-1 and CFPAC-1 cell lines. (F) IGV snapshots showing H3K18la-binding signals in the TSS region of ACAT2 in different groups. (G) ChIP-qPCR analysis of the indicated promoters was performed using antibodies against H3K18la in PANC-1 and CFPAC-1 cells treated with or without 20 mM oxamate for 24 hours. Two-tailed unpaired t test. (H) Immunoblotting of ChIP assays illustrating the binding sites at the ACAT2 promoters against H3K18la. (I, J) Representative images (I) and quantification (J) of ACAT2 levels visualised by immunofluorescence staining in tumour and normal tissues (n=174). Scale bar: left panel, 100 µm; right panel, 20 µm. Two-tailed paired t-test. (K) Correlation between H3K18la levels and ACAT2 expression (n=174). Spearman correlation analysis. (L, M) Western blot analysis of the indicated proteins from PANC-1 cells with different treatments. Lactate 20 mM, C646 100 mM or TSA 1 mM for 24 hours. (N) Western blot analysis of EP300, H3K18la and ACAT2 in PANC-1 cell lines. (O) ChIP-qPCR analysis of the indicated promoters was performed using antibodies against H3K18la in PANC-1 and CFPAC-1 cells with different treatments. Two-tailed unpaired t-test. (P) Immunoblotting of ChIP assay results illustrating the binding sites at the ACAT2 promoters against H3K18la. Data are represented as the mean±SD. *p<0.05; **p<0.01. PDAC, pancreatic ductal adenocarcinoma; TSA, trichostatin a.

pancreatic cancer cells *in vitro* (online supplemental figure S2I,J).

ACAT2 induces MTCH2 acetylation and enhances its protein stability

Given that ACAT2 converts two molecules of acetyl-CoA into acetoacetyl-CoA and CoA during ketogenesis,[17] we investigated its role as an acetyltransferase. Co-immunoprecipitation (Co-IP) assays following mass spectrometry (MS) identified mitochondrial carrier homolog 2 (MTCH2) as a critical protein interacting with ACAT2 (figure 3A,B). Co-IP experiments and GST pull-down assay revealed a specific interaction between ACAT2 and MTCH2 (figure 3C–E, online supplemental figure S3A–C). We generated various truncated forms of MTCH2 and assessed their coprecipitation with ACAT2. Flag-ACAT2 failed to coprecipitate GST-tagged peptide containing amino acids 181–230 and 231–303 of MTCH2, indicating the specific interaction between ACAT2 and amino acids 1–77 and 78–180 of MTCH2 (figure 3F).

Next, we investigated whether MTCH2 serves as an acetylation substrate for ACAT2. ACAT2 knockout led to a notable decrease in the basal acetylation levels of MTCH2, which was restored on reintroducing CRISPR Cas9-resistant Flag-tagged ACAT2 into the knockout cells (figure 3G,H, online supplemental figure S3D,E). *In vitro* acetylation assays demonstrated efficient acetylation of GST-MTCH2 in the presence of acetyl-CoA, confirming that ACAT2 directly acetylates MTCH2 (figure 3I). To identify acetylation sites on MTCH2, we used PhosphoSitePlus prediction tools[18] and mutated predicted lysine residues (K100, K122, K158, K293) to arginine (R) to pinpoint ACAT2-catalysed acetylation sites (figure 3J). HA-tagged MTCH2 mutants were transfected into HEK 293 T cells, revealing that both K100R and K158R mutations significantly reduced acetylation levels, while the double mutant MTCH2-K100R/K158R (MTCH2-2KR) exhibited minimal acetylation (figure 3K,L).

We next assessed whether ACAT2 influences MTCH2 stability. Cycloheximide (CHX) treatment revealed that ACAT2 knockout accelerated MTCH2 degradation (figure 3M, online supplemental figure S3F). Variations in MTCH2 protein were lessened by treatment with the proteasome inhibitor MG132 between control and ACAT2 knockout groups (online supplemental figure S3G), suggesting that ACAT2 inhibits MTCH2 proteasomal degradation. These findings prompted an investigation into whether ACAT2-mediated acetylation affects MTCH2-ubiquitin binding. We discovered that the K100R mutation increased MTCH2 ubiquitination (figure 3N). Acetylation-mimetic mutants (MTCH2-K100Q, MTCH2-K158Q and MTCH2-K100Q/K158Q (MTCH2-2KQ)) revealed that only K100Q mutant significantly reduced MTCH2 ubiquitination (figure 3O). Furthermore, when we assessed MTCH2 ubiquitination with different ubiquitin mutants, mutations at K29R and K48R (K-R) diminished MTCH2 ubiquitination, with the K48R mutant resulting in a more pronounced reduction (figure 3P). In summary, our data suggest that ACAT2-mediated acetylation of K100 in MTCH2 inhibits its degradation by obstructing K29 and K48-linked ubiquitination.

Lactate/H3K18la/ACAT2/MTCH2 forms a positive feedback loop in pancreatic cancer

MTCH2, a member of the membrane protein insertase family, is capable of inserting proteins into human mitochondria.[19] Prior research has demonstrated that loss of MTCH2 enhances mitochondrial OXPHOS while reducing lactate production in progenitor cells.[20] In light of this, we hypothesised that the stability of MTCH2, mediated by ACAT2 acetylation, diminishes mitochondrial respiration and facilitates lactate production.

MTCH2 knockdown increased spare respiratory capacity (SRC), as indicated by elevated oxygen consumption rate (figure 4A,B). Besides changes in mitochondrial function, changes in mitochondrial structure were detected by electron microscopy, revealing that the mitochondria of MTCH2-deficient PANC-1 cells were significantly elongated (online supplemental figure S4A). Correspondingly, this increase in OXPHOS activity was associated with decreased lactate production in MTCH2-deficient cells (figure 4C). After ACAT2 knockdown, we observed results consistent with MTCH2 knockdown. Importantly, MTCH2 overexpression reversed the effects of ACAT2 knockdown (figure 4D–F). These findings confirm that ACAT2 decreases OXPHOS activity by enhancing the stability of MTCH2, ultimately promoting lactate production. ChIP-qPCR showed reduced H3K18la levels at the ACAT2 promoter in ACAT2-knockdown cells, while MTCH2 overexpression restored the diminished H3K18la enrichment (figure 4G). Furthermore, knockdown of MTCH2 led to significant reductions in both Pan Kla and H3K18la levels, which were reversed by MTCH2 overexpression (online supplemental figure S4B). Similar results caused by ACAT2 knockdown were also rescued by overexpression of MTCH2 (figure 4H). Collectively, these results support the presence of a lactate/H3K18la/ACAT2/MTCH2 positive feedback loop, which drives ACAT2 upregulation and metabolic reprogramming of pancreatic cancer cells (figure 4I).

A*cat2* deficiency induces an immunosuppressive tumour-associated macrophage compartment and CD8$^+$ T-cell dysfunction in pancreatic cancer tumour microenvironment

To investigate ACAT2's role in pancreatic cancer growth *in vivo*, we constructed *Acat2* wild-type (*Acat2*^{WT}) and knockout (*Acat2*^{KO}) Panc02 cell lines and subcutaneously inoculated them into immune-deficient NCG and BALB/c nude mice. We observed tumour growth inhibition in *Acat2*^{KO} tumours (figure 5A–D, online supplemental figure S5A–C). To validate whether ACAT2 modulates tumour immune response additionally, we injected *Acat2*^{WT} and *Acat2*^{KO} Panc02 cells into C57BL/6 J mice. While *Acat2* knockout retarded tumour growth in BALB/c nude and NCG mice, *Acat2*^{KO} tumours showed even more significant growth inhibition in C57BL/6 J mice (figure 5E–G), suggesting reduced growth due to both tumour cell effects and immune response changes. To assess ACAT2's impact on the immune landscape, we used Panc02 and KPC cells expressing ovalbumin (OVA) to establish pancreatic orthotopic tumours. *Acat2*^{KO} tumours exhibited significantly lower tumour burden compared with *Acat2*^{WT} tumours (online supplemental figure S5D–J). Mass cytometry by time-of-flight analysis was used to reveal ACAT2's role in the tumour microenvironment (TME) (figure 5H).

We established a 42-marker panel to determine immune cell lineages, identifying 29 unique clusters grouped into 12 populations (figure 5I). The distributions of these clusters, populations and markers were visualised via t-SNE plots (figure 5J–K, online supplemental figure S5K). Decreased infiltration of M2-like tumour-associated macrophages (TAMs), increased M1-like TAMs and CD8$^+$ T cells were observed in the *Acat2*^{KO} group (figure 5L, online supplemental figure S6A). Additionally, we noticed an increase, though not significant, in the memory T cell population. These results suggest ACAT2 deletion shifts TME towards a more antitumour immune profile. Multiplex

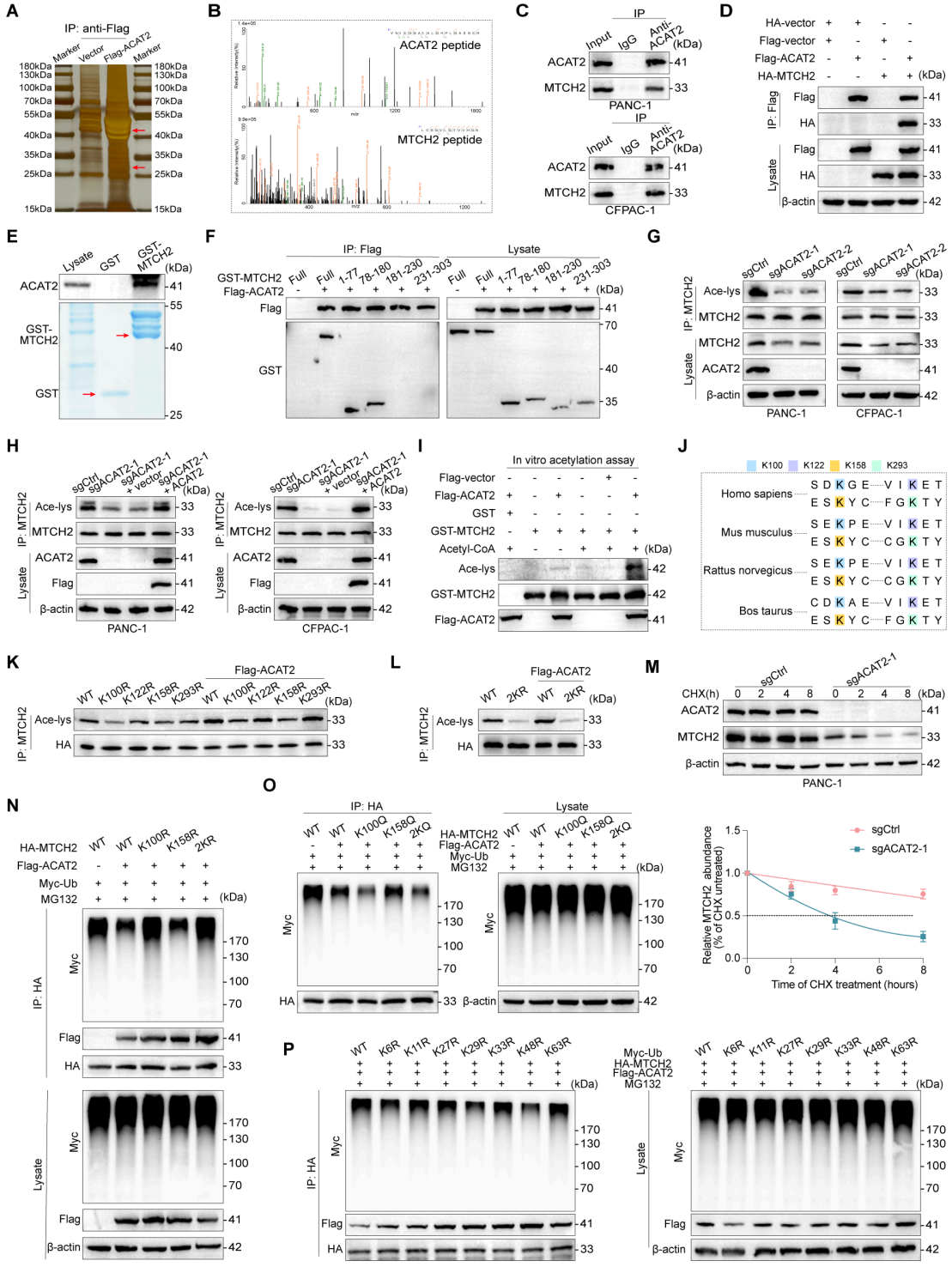

Figure 3 ACAT2 induces MTCH2 acetylation and enhances its protein stability. (A, B) Sliver staining and mass spectrum analysis of ACAT2 interacting proteins. (C) Co-precipitation of endogenous MTCH2 with ACAT2 from PANC-1 and CFPAC-1 cells. (D) Co-precipitation of exogenous MTCH2 with ACAT2 from HEK 293T cells. (E) HEK 293T cell lysates were incubated with purified GST-MTCH2 (31–170 amino acids), and bound ACAT2 was detected by western blot using anti-ACAT2. (F) Co-precipitation of GST-tagged MTCH2 truncats with Flag-ACAT2 from HEK-293T cells. (G, H) Acetylation of MTCH2 in PDAC cells detected by western blot after co-precipitation. Flag-tagged ACAT2 (H) was co-expressed in ACAT2 knockout cell lines. IP with MTCH2 antibody and IB with Ace-lys antibody. (I) *In vitro* MTCH2 acetylation assay. Purified GST-MTCH2 was incubated with Flag-ACAT2 immunoprecipitated from HEK 293T cells, in the presence or absence of acetyl-CoA. (J) Alignment of MTCH2 amino acid sequence from various species. (K, L) Acetylation of MTCH2 mutants expressed in HEK 293T cells. HA-tagged MTCH2 mutants cells were transfected with or without Flag-ACAT2. (M) MTCH2 protein expression in ACAT2-knockout or control PANC-1 cells. Bottom: The dashed line intersects the degradation curves at the half-life. (N, O) Co-precipitation of ubiquitylated proteins with HA-MTCH2. HA-MTCH2 was immunoprecipitated by anti-HA from HEK 293T cells transiently expressing HA-tagged WT MTCH2 or each of the MTCH2 mutants, and co-precipitated ubiquitylated proteins were detected using anti-Myc. (P) HEK 293T cells were coexpressed with different vectors. IP and IB with indicated antibodies. IB, immunoblotting; IP, immunoprecipitation; PDAC, pancreatic ductal adenocarcinoma.

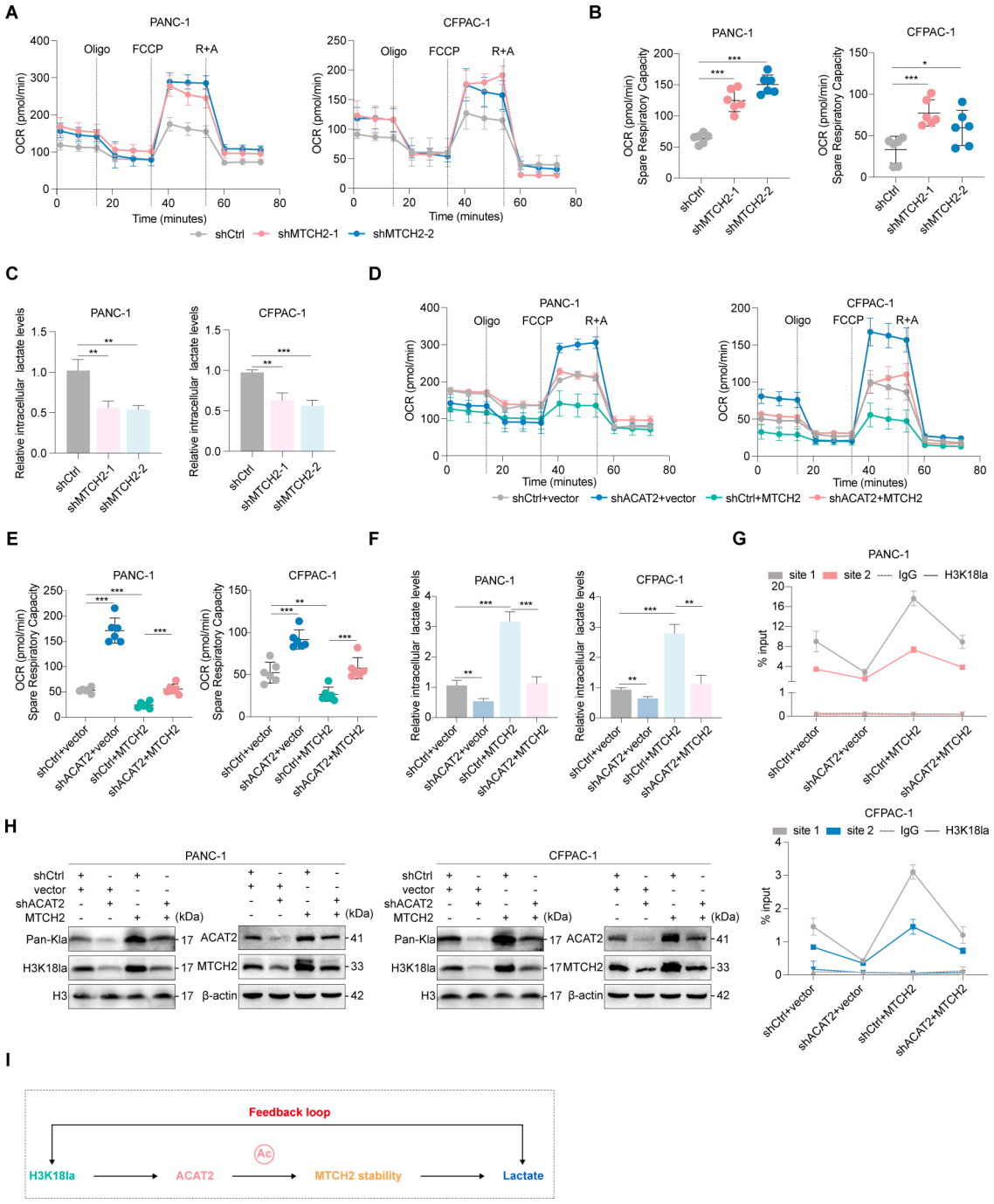

Figure 4 Lactate/H3K18la/ACAT2/MTCH2 forms a positive feedback loop in pancreatic cancer. (A, B) OCR in MTCH2-knockdown or control PDAC cells. Two-tailed unpaired t test. (C) Intracellular lactate levels in PDAC cells with or without MTCH2 knockdown. Two-tailed unpaired t-test. (D, E) OCR in ACAT2 knockdown, ACAT2 knockdown co-transfected with MTCH2 overexpression or control PDAC cells. Two-tailed unpaired t-test. (F) Intracellular lactate levels in ACAT2 knockdown, ACAT2 knockdown co-transfected with MTCH2 overexpression or control PDAC cells. Two-tailed unpaired t-test. (G) qChIP analysis of the indicated promoters was performed using antibodies against H3K18la in ACAT2 knockdown, ACAT2 knockdown co-transfected with MTCH2 overexpression or control PDAC cells. (H) Western blot analysis shows the levels of indicated proteins in ACAT2 knockdown, MTCH2 overexpression, ACAT2 knockdown co-transfected with MTCH2 overexpression or control PDAC cells. (I) Schematic illustration of a positive feedback loop between H3K18la and ACAT2 in pancreatic cancer. Data are represented as the mean±SD. *p<0.05; **p<0.01; ***p<0.001. PDAC, pancreatic ductal adenocarcinoma.

immunohistochemistry (mIHC) of human pancreatic cancer tissue specimens revealed significantly higher M2-like TAMs and lower CD8$^+$ T cell infiltration in tumours with high ACAT2 expression (figure 5M). Given that M2-like TAMs promote immune suppression,[21 22] reduced *Acat2*^{KO} tumour growth may result from alterations in the TAM compartment.

Flow cytometry analysis of immune cells revealed that *Acat2*^{KO} tumours had significantly more tumour-infiltrating CD8$^+$ T cells, higher proportions of granzyme B (GZMB)$^+$ and interferon-gamma (IFN-γ)$^+$ CD8$^+$ T cells, and fewer M2-like TAMs (CD11b$^+$F4/80$^+$CD206^{high}) (figure 5N,O, online supplemental figure S6B–E). Also, the subcutaneous tumour

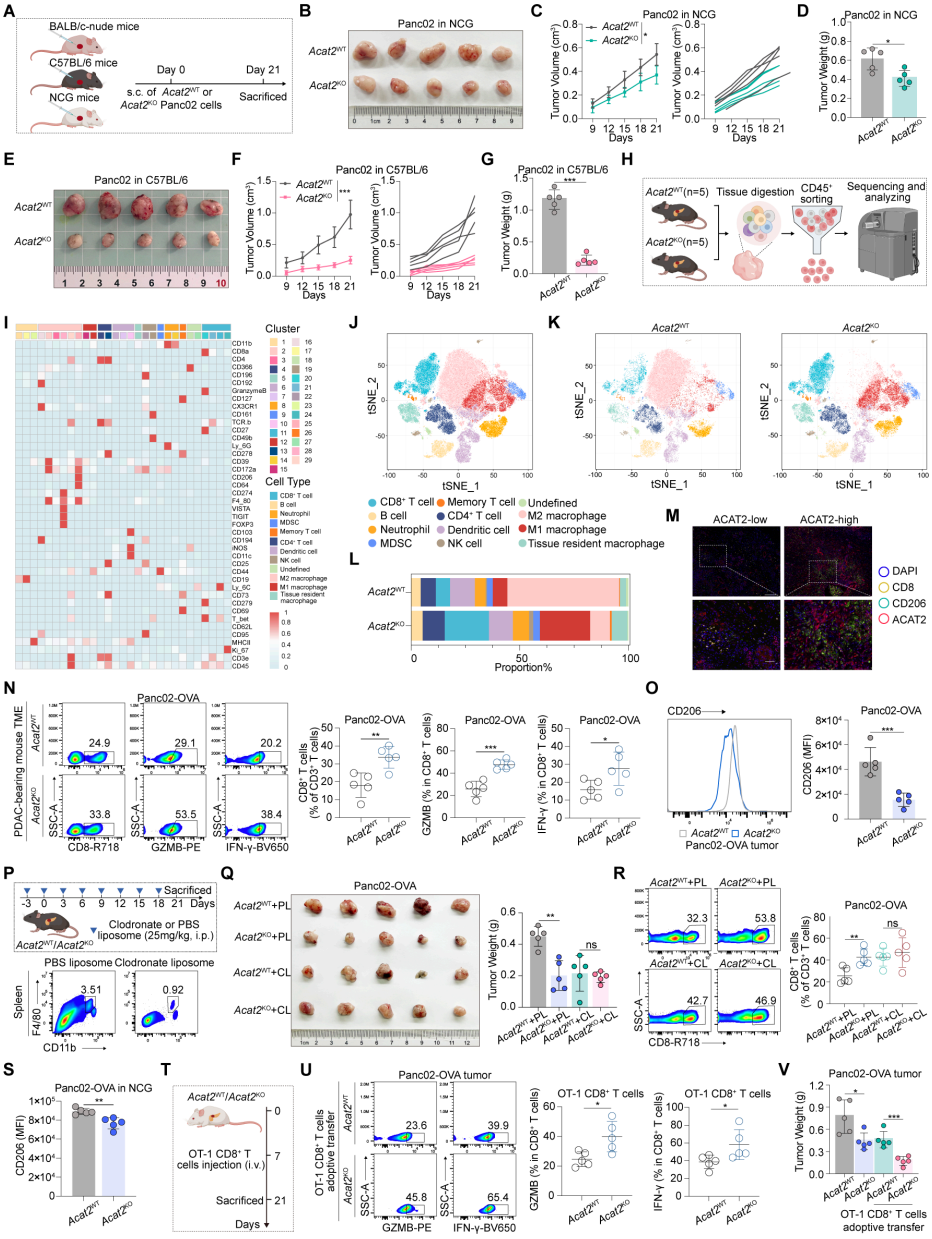

Figure 5 *Acat2* deficiency induces an immunosuppressive tumour-associated macrophage compartment and CD8$^+$ T-cell dysfunction in pancreatic cancer tumour microenvironment. (A) Diagram outlining the approach to testing inhibition of ACAT2 in immune-competent and immune-deficient tumour-bearing mice. (B–D) The effects of *Acat2* knockout on Panc02 tumour growth were evaluated in NCG mice (n=5 mice per group). Representative images of tumours (B), growth curves (C) and tumour weight (D) for indicated groups were presented. Two-tailed unpaired t-test. (E–G) The effects of *Acat2* knockout on Panc02 tumour growth were evaluated in C57BL/6 mice (n=5 mice per group). Representative images of tumours (E), growth curves (F) and tumour weight (G) for indicated groups were presented. Two-tailed unpaired t test. (H) Schematic illustration of CyTOF data acquisition (n=5 per group). (I) Heatmap of the expression of the 42 markers for immune cell lineage in the 12 cell populations obtained by merging of the 29 meta-clusters. (J, K) t-SNE plot of Panc02-OVA tumour-infiltrating leukocytes subpopulations overlaid with colour-coded clusters. (L) Frequency of tumour-infiltrating immune cell clusters in the *Acat2*^{WT} and *Acat2*^{KO} group (n=5 per group). (M) Representative mIHC images of ACAT2, CD8 and CD206 in human PDAC tissues. Scale bar: upper, 100 µm; bottom, 20 µm. (N, O) 5×10^5*Acat2*^{WT} or *Acat2*^{KO} Panc02-OVA cells were pancreatic orthotopic injected into C57BL/6 mice (n=5). Representative flow cytometry plots and quantification of tumour-infiltrating CD8$^+$ T cells, granzyme B$^+$CD8$^+$ T cells, IFN-γ$^+$CD8$^+$ T cells (N) and M2-like macrophages (CD206$^+$) (O) for the indicated groups were presented. Two-tailed unpaired t-test. (P) Experimental setup and flow cytometry validation (bottom) of orthotopic pancreatic tumour-bearing C57BL/6 mice with depletion of macrophages. (Q, R) 5×10^5*Acat2*^{WT} or *Acat2*^{KO} Panc02-OVA cells were pancreatic orthotopic injected into C57BL/6 mice with or without macrophages depletion (n=5). Representative images of tumours (Q) and flow cytometry of tumour-infiltrating CD8$^+$ T cells for the indicated groups (R) were presented. Two-tailed unpaired t test. (S) 5×10^5*Acat2*^{WT} or *Acat2*^{KO} Panc02-OVA cells were pancreatic orthotopic injected into NCG mice. Quantification of tumour-infiltrating M2-like macrophages was presented. Two-tailed unpaired t test. (T) The schematic of the OT-1 CD8$^+$ T cells treatment schedule. (U, V) 5×10^5*Acat2*^{WT} or *Acat2*^{KO} Panc02-OVA cells were pancreatic orthotopic injected into NCG mice with or without OT-1 CD8$^+$ T cells adoptively transferred. Tumour-infiltrating activated CD8$^+$ T cells were assessed by flow cytometry (U) and tumour weight (V) was shown. Two-tailed unpaired t test. Data are represented as the mean±SD. *p<0.05; **p<0.01; ***p<0.001. CyTOF, cytometry by time-of-flight; mIHC, multiplex immunohistochemistry; ns, not significant; OVA, ovalbumin; PDAC, pancreatic ductal adenocarcinoma; s.c., subcutaneous;.

implantation model with KPC2 cells showed results consistent with those observed in Panc02-OVA and KPC-OVA cells (online supplemental figure S6F–I). These results suggest that ACAT2 in tumour cells promotes an immunosuppressive TME by supporting M2-like TAM polarisation and suppressing $CD8^+$ T-cell function. To determine whether the reduced tumour growth in *Acat2*^{KO} tumours was macrophage-dependent, we depleted macrophages in mice using clodronate liposomes. Macrophage depletion restored tumour growth in *Acat2*^{KO} tumours, confirming that ACAT2's effects on tumour progression are partially mediated by TAMs (figure 5P–R, online supplemental figure S6J,K).

Despite no dramatic difference in tumour growth between *Acat2*^{WT} and *Acat2*^{KO} tumours in NCG mice, *Acat2*^{KO} tumours still showed a significantly reduced proportion of M2-like TAMs (figure 5S, online supplemental figure S6L). Since M2-like TAMs suppress T-cell function,[23] we hypothesise that reduced M2-like TAMs in *Acat2*^{KO} tumours contribute to increased $CD8^+$ T cell infiltration. We then injected OT-1 $CD8^+$ T cells into orthotopic tumour-bearing NCG mice to test this. The tumour growth difference between *Acat2*^{WT} and *Acat2*^{KO} tumours was enhanced by OT-1 $CD8^+$ T cell transfer, and *Acat2*^{KO} tumours displayed higher percentages of activated $CD8^+$ T cells (figure 5T–V, online supplemental figure S6M). Together, these findings demonstrate that ACAT2 deficiency reshapes the TME by suppressing M2-like TAMs, which enhanced $CD8^+$ T-cell activity, ultimately reducing tumour growth.

ACAT2-induced increase in cholesterol delivery to TAMs causes an immunosuppressive TME

To mimic the influence of pancreatic cancer cells on macrophages within the TME, we cultured bone marrow-derived macrophages (BMDMs) in tumour cell-derived conditioned medium (TCM) from mouse pancreatic cancer cells to induce TAM-like traits (figure 6A). Flow cytometry showed that TAMs exposed to TCM from *Acat2*^{KO} cells reduced CD206 expression, while TCM from *Acat2*^{OE} cells increased M2-like TAMs (figure 6B, online supplemental figure S7A). RNA-seq demonstrated that TAMs cultured in *Acat2*^{KO} TCM downregulated M2-like signature genes and upregulated M1-like signatures (figure 6C, online supplemental figure S7B). These results were validated through qRT-PCR (online supplemental figure S7C,D), showing that ACAT2 deficiency in tumour cells suppresses M2 polarisation. TAMs treated with TCM from *Acat2*^{KO} cells showed reduced secretion of the immunosuppressive cytokines IL-10 and TGF-β, while TAMs from *Acat2*^{OE} TCM increased their secretion (figure 6D, online supplemental figure S7E). Additionally, TAMs cultured in TCM from *Acat2*^{KO} cells were less effective in suppressing $CD8^+$ T-cell activity (figure 6E,F, online supplemental figure S7F–H). These findings confirm that overexpression of ACAT2 in tumour cells enhances M2 polarisation, contributing to the immunosuppressive TME.

We next explored the mechanism by which ACAT2 influences M2 polarisation. Despite ACAT2's effect on intracellular lactate levels, extracellular lactate levels remained unchanged across *Acat2*^{KO}, *Acat2*^{OE} and *Acat2*^{WT} cells (online supplemental figure S7I). Since ACAT2 converts acetyl-CoA to acetoacetyl-CoA, a precursor of HMG-CoA in the mevalonate pathway that drives cholesterol biosynthesis, we aim to explore cholesterol's potential role in this process. Given TAMs and tumour cells as major cholesterol consumers in the TME,[24 25] we hypothesised that ACAT2 may affect the TME by modulating cholesterol synthesis. Filipin staining showed reduced cholesterol in *Acat2*^{KO} cells and elevated levels in *Acat2*^{OE} cells (figure 6G, online supplemental figure S7J–L). Cholesterol supplementation promoted M2 polarisation, while methyl-β-cyclodextrin (MβCD), which depletes membrane cholesterol, reduced CD206 expression (online supplemental figure S7M,N). TAMs cultured in TCM from *Acat2*^{KO} cells also showed reduced cholesterol levels (figure 6H, online supplemental figure S7O,P). We then explored the secretion of cholesterol by tumour cells. Cholesterol is typically transported as lipoproteins, primarily synthesised in the liver and intestine, suggesting that tumour cells may secrete cholesterol in another form.[26] Given that tumour cells release cholesterol-rich small extracellular vesicles (sEVs),[27] we speculated that ACAT2 promotes cholesterol secretion via sEVs. sEVs extracted from Panc02-OVA cells displayed typical morphology with a diameter of 50–200 nm (online supplemental figure S8A–C). Cholesterol content was significantly higher in sEVs from *Acat2*^{OE} cells, while *Acat2*^{KO} cells produced fewer cholesterol-loaded sEVs (figure 6I). Addition of sEVs promoted M2 polarisation in a dose-dependent manner (online supplemental figure S8D), with BMDMs treated with *Acat2*^{OE} sEVs showing higher cholesterol content and enhanced M2-like polarisation (figure 6J–L, online supplemental figure S8E,F). Importantly, TAMs treated with *Acat2*^{KO} cell-derived sEVs were less effective in suppressing $CD8^+$ T-cell activity (figure 6M,N). Meanwhile, sEVs from *Acat2*^{KO} cells moderately suppressed tumour growth, with decreased M2-like TAMs and increased activated $CD8^+$ T cells (figure 6O,P, online supplemental figure S8G–I). These findings indicate that ACAT2-mediated cholesterol is delivered to TAMs via sEVs, promoting M2 polarisation and contributing to an immunosuppressive TME. To confirm sEV-mediated cholesterol transfer, we employed amiloride and EIPA (both macropinocytosis inhibitors) and chlorpromazine (clathrin-dependent endocytosis inhibitor). Here, PKH67-labelled sEVs could be internalised by TAMs, and chlorpromazine most significantly reduced CD206 levels in TAMs (figure 6Q, online supplemental figure S8J,K). Also, TAMs cultured with TCM from GW4869 (an inhibitor of sEV biogenesis) pretreated cells showed decreased CD206 expression (figure 6R, online supplemental figure S8L,M). PI3K/Akt/mTOR, JAK/STAT3 and JAK/STAT6 pathways play key roles in M2 polarisation.[28 29] We cultured BMDMs with TCM or sEVs from *Acat2*^{KO} or *Acat2*^{OE} tumour cells and found increased phosphorylation of AKT, STAT3 and STAT6 in TAMs treated with TCM or sEVs from *Acat2*^{OE} tumour cells. This effect was blocked by chlorpromazine, confirming ACAT2-mediated, cholesterol-driven M2 polarisation (figure 6S).

In summary, our findings suggest that the positive feedback loop within pancreatic cancer cells drives excessive ACAT2 upregulation, promoting cholesterol secretion via sEVs, inducing TAMs M2 polarisation, and establishing an immunosuppressive TME.

Targeted degradation of *Acat2* or *Acat2* deficiency sensitises ICB therapy in pancreatic cancer

ICB therapy has emerged as an effective cancer immunotherapy.[30 31] Many immune cells overexpress inhibitory molecules like PD-1, dampening antitumour immune responses. According to our research, ACAT2 is essential for regulating the TME, particularly through its influence on TAMs and $CD8^+$ T cells, making it a potential target for enhancing ICB efficacy.

We observed more M2-like TAMs in *Acat2*^{WT} tumours and increased $CD8^+$ T cells in *Acat2*^{KO} tumours, suggesting that targeting ACAT2 may enhance anti-PD-1 therapy efficacy. Indeed, combining an anti-PD-1 antibody (αPD-1) with *Acat2*^{KO}

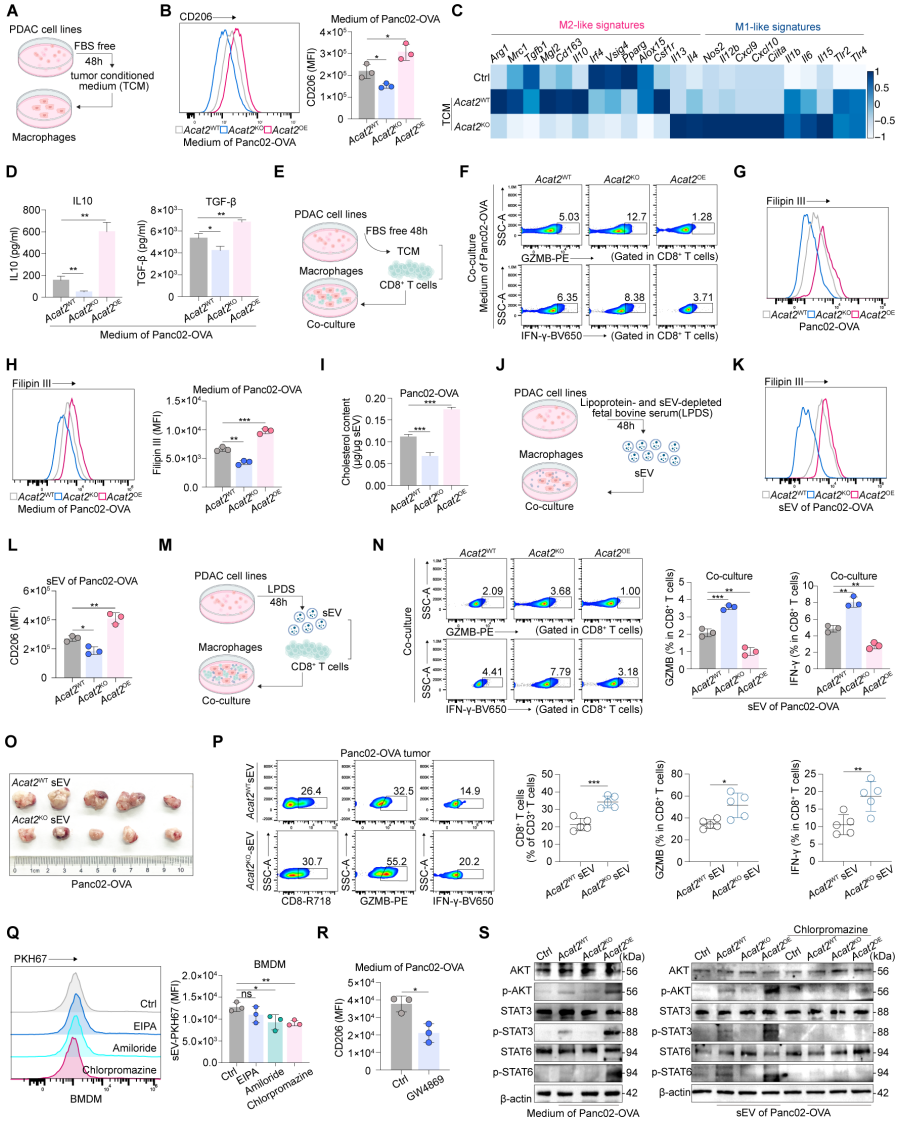

Figure 6 ACAT2-induced increase in cholesterol delivery to TAMs causes an immunosuppressive TME. (A) Schematic of *in vitro* macrophage system. (B) BMDMs isolated from C57BL/6 mice were cultured in DMEM medium with 20 ng/mL M-CSF. On day 6, cells were treated with TCM from Panc02-OVA (A) for 48 hours. The MFI of M2-like macrophages in each group of macrophages was detected by flow cytometry (n=3). Two-tailed unpaired t-test. (C) Heatmap showing the expression levels of marker genes in the identified macrophage clusters from indicated groups. (D) The IL-10 and TGF-β levels of macrophages cultured with FBS-free medium for 24 hours, which were prior treated with TCM from Panc02-OVA and fresh medium at a ratio of 1:1 for 24 hours using ELISA. Two-tailed unpaired t-test. (E) Schematic of *in vitro* co-culture system. (F) Flow cytometry of activated $CD8^+$ T cells co-cultured with macrophages from (E). (G) Filipin III staining of *Acat2*^{WT}, *Acat2*^{KO} and *Acat2*^{OE} Panc02-OVA cells were detected by flow cytometry (n=3). (H) BMDMs isolated from C57BL/6 mice were cultured in DMEM medium with 20 ng/mL M-CSF. On day 6, cells were treated with TCM (A) for 48 hours. The Filipin III staining in each group of macrophages was detected by flow cytometry (n=3). Two-tailed unpaired t-test. (I) Cholesterol content of Panc02-OVA cells-derived sEVs. Two-tailed unpaired t test. (J) Schematic of *in vitro* co-culture system. (K, L) BMDMs isolated from C57BL/6 mice were cultured in DMEM medium with 20 ng/mL M-CSF. On day 6, cells were treated with sEVs for 48 hours. The Filipin III staining (K) and the quantification of M2-like MFI (L) in each group of macrophages were detected by flow cytometry (n=3). Two-tailed unpaired t test. (M) Schematic of *in vitro* co-culture system. (N) Flow cytometry of activated $CD8^+$ T cells co-cultured with macrophages from (M). Two-tailed unpaired t test. (O, P) Pancreatic orthotopic tumour-bearing mice were intravenously injected with 100 μg sEVs on days 7 and 14 after tumour cell inoculation. Representative images of tumours (O), representative flow cytometry plots and quantification of tumour-infiltrating $CD8^+$ T cells, granzyme B^+CD8^+ T cells and IFN-γ^+CD8^+ T cells (P) for the indicated groups were presented. Two-tailed unpaired t test. (Q) BMDMs cultured in medium with 20 ng/mL M-CSF for 6 days were treated with 2 μg PKH67-labelled sEVs±amiloride (10 mM), chlorpromazine (10 mM) or EIPA (5 mM) for 12 hours. The MFI of PKH67 was assessed by flow cytometry. Two-tailed unpaired t-test. (R) BMDMs cultured in medium with 20 ng/mL M-CSF for 6 days were treated with 2 μg sEVs isolated from TCM derived from Panc02-OVA. The cells were cultured with LPDS±10 μM GW4869 for 2 days. The MFI of CD206 was assessed by flow cytometry. Two-tailed unpaired t test. (S) BMDMs were cultured in medium with 20 ng/mL M-CSF for 6 days, followed by a medium containing LPDS±chlorpromazine (10 mM) and 2 μg of sEVs from *Acat2*^{WT}, *Acat2*^{KO} and *Acat2*^{OE} Panc02-OVA cells for 48 hours. Indicated proteins of macrophages were detected by western blot. Data are represented as the mean±SD. *p<0.05; **p<0.01; ***p<0.001. BMDM, bone marrow-derived macrophages; DMEM, dulbecco's modified eagle's medium; LPDS, lipoprotein- and sEV-depleted fetal bovine serum; M-CSF, macrophage colony-stimulating factor; MFI, mean fluorescence intensity; sEVs, small extracellular vesicles; TAMs, tumour-associated macrophages; TCM, tumour cell-derived conditioned medium; TME, tumour microenvironment.

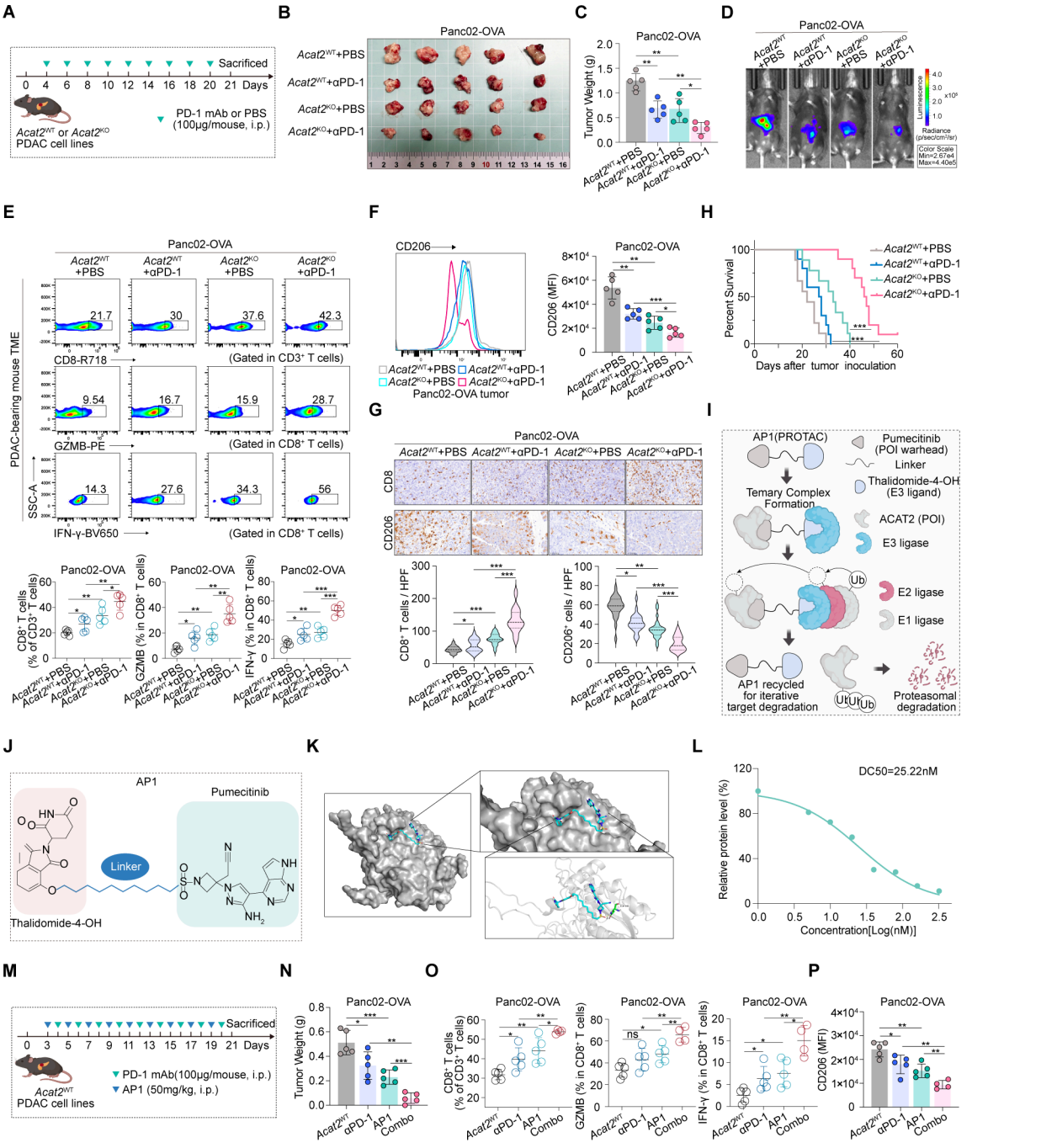

Figure 7 Targeted degradation of *Acat2* or *Acat2* deficiency sensitises ICB therapy in pancreatic cancer. (A) The schematic of the αPD-1 treatment schedule. (B–D) 5×10^5 *Acat2*^{WT} or *Acat2*^{KO} Panc02-OVA cells were pancreatic orthotopic injected into C57BL/6 mice with or without αPD-1 treatment (n=5). Representative images of tumours (B), tumour weight (C) and bioluminescence images (D) for the indicated groups were presented. One-way ANOVA. (E) Percentage of tumour-infiltrating CD8$^+$ T cells, granzyme B$^+$CD8$^+$ T cells, IFN-γ$^+$CD8$^+$ T cells by flow cytometry. One-way ANOVA. (F) Representative flow cytometry plots and quantification of M2-like macrophages (CD206$^+$). One-way ANOVA. (G) IHC staining of CD8$^+$ and CD206$^+$ cells in tumour. Number of CD8-positive cells and CD206-positive cells per HPF was counted in tumour sections from each group. Five random HPFs were selected for analysis on each slide. Scale bar, 50 μm. One-way ANOVA. (H) Survival curve. Log rank test. (I) Schematic illustration of the design strategy of ACAT2 PROTAC. (J) Predicted binding model of compound pumecitinib with ACAT2. (K) Chemical structures of the PROTAC AP1. (L) DC50 of Panc02 cells treated with AP1 with various concentrations for 24 hours. (M) The schematic of the AP1 and αPD-1 treatment schedule. (N–P) 5×10^5 *Acat2*^{WT} Panc02-OVA cells were pancreatic orthotopic injected into C57BL/6 mice with or without AP1/αPD-1 treatment (n=5). Tumour weight (N), percentage of CD8$^+$ T cells, GZMB$^+$CD8$^+$ T cells, IFN-γ$^+$CD8$^+$ T cells (O) and quantification of CD206 (P) for the indicated groups were presented. One-way ANOVA. Data are represented as the mean±SD. *p<0.05; **p<0.01; ***p<0.001. ANOVA, analysis of variance; HPF, High Power Field; ICB, immune checkpoint blockade; IHC, immunohistochemistry; PROTAC, proteolysis-targeting chimaera.

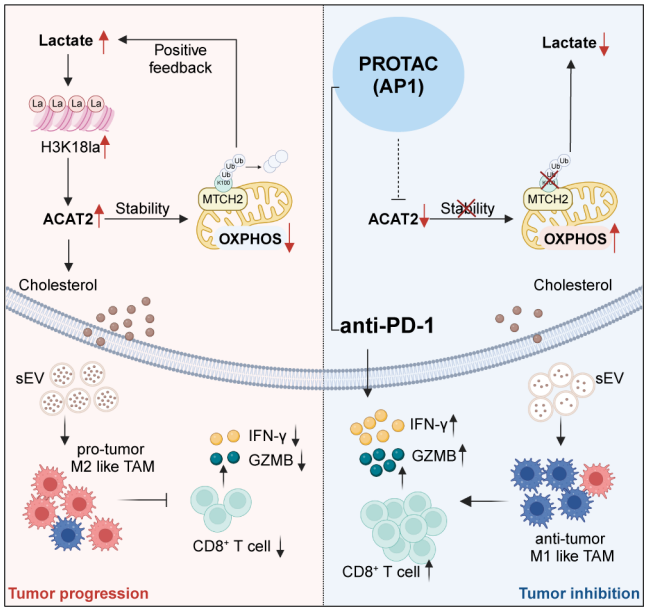

Figure 8 Schematic cartoon illustrating the roles of histone lactylation-induced ACAT2/MTCH2/lactate positive feedback loop in orchestrating cholesterol-mediated immunosuppressive reprogramming in pancreatic cancer. PROTAC, proteolysis-targeting chimaera; sEVs, small extracellular vesicles; TAM, tumour-associated macrophages.

resulted in greater tumour growth inhibition and extended survival compared with either treatment alone (figure 7A–D and H and online supplemental figure S9A–C). Consistent with these results, the administration of αPD-1 in the *Acat2*^{KO} group reduced M2-like TAMs and increased CD8$^+$ T cell infiltration (figure 7E,F, online supplemental figure S9D,E). IHC confirmed that *Acat2*^{KO} combined with anti-PD-1 therapy increased CD8$^+$ T cell infiltration, while decreasing CD206$^+$ M2-like TAMs (figure 7G). This shift in immune cell populations supports the hypothesis that ACAT2 deletion reprograms the TME, sensitising tumours to ICB.

Given the strong effect of *ACAT2*^{KO} combined with αPD-1, we designed a specific PROTAC degrader to degrade ACAT2 *in vivo*. PROTACs are heterobifunctional molecules with a warhead targeting the protein of interest (POI), a ligand for E3 ligase and a linker that joins them. The E3 ligase and POI are engaged by a PROTAC to form a ternary complex, leading to ubiquitination and proteasomal degradation of the POI. Using surface plasmon resonance, we identified pumecitinib as a compound with high affinity for ACAT2. The compound was connected with a CRBN (E3 ligase) ligand using a chemical linker, forming our PROTAC of ACAT2, named AP1 (figure 7I–K, online supplemental figure S9F). AP1 showed strong degradation efficacy with a DC50 value of 25.22 nM in Panc02-OVA cells (figure 7L, online supplemental figure S9G). To further verify the targeting specificity of AP1, we performed proteomics analysis on Panc02-OVA cells treated with AP1. Compared with the control group, the AP1-treated group exhibited the most significant degradation of ACAT2 protein (online supplemental figure S9H). CCK-8 assays confirmed AP1's inhibitory effect on Panc02-OVA cell growth *in vitro* (online supplemental figure S9I). Additionally, we observed that AP1 treatment downregulated MTCH2 protein expression, while upregulating mitochondrial SRC and downregulating intracellular lactate levels (online supplemental figure S9I–M). These results collectively validate that AP1 exerts regulatory effects consistent with those of *Acat2*^{KO}. Next, we demonstrated that *in vivo* degradation of *Acat2* by AP1 significantly inhibited tumour growth at a dose of 50 mg/kg (online supplemental figure S9N,O). In order to verify the toxicity of AP1 in mice, H&E staining was performed on the heart, liver, spleen, lung and kidney of the tumour-bearing mice (online supplemental figure S9P). No obvious damage was found, which proved the safety of AP1. *In vivo*, AP1 treatment significantly inhibited Panc02-OVA tumour growth. The combination of AP1 with αPD-1 exhibited the most potent tumour inhibition and significantly increased antitumour immunity (figure 7M–P, online supplemental figure S10A–C). Together, our data suggest that targeting ACAT2 enhances the efficacy of PD-1 blockade therapy in pancreatic cancer by reducing immunosuppressive M2-like TAMs and increasing the presence of tumour-infiltrating CD8$^+$ T cells.

DISCUSSION

Histone lactylation, an epigenetic modification regulated by intracellular lactate levels, affects gene transcription, macrophage polarisation and somatic cell reprogramming.[9 32 33] Our study uncovered a lactate/H3K18la/ACAT2/MTCH2 positive feedback loop that not only exacerbates lactate accumulation within pancreatic cancer cells but also promotes tumour progression. Interruption of this feedback loop through ACAT2 inhibition led to decreased H3K18la levels, restoration of MTCH2 degradation and a reduction in lactate production. This highlights the potential of targeting this vicious cycle as a therapeutic strategy for pancreatic cancer.

Emerging evidence highlights the interplay between histone modifications and energy metabolism.[8] Metabolites from the tricarboxylic acid cycle and glycolysis, such as acetyl-CoA and lactate, serve as substrates for histone modifications.[34] Increase of these substrates from metabolic reprogramming may lead to significant changes in histone modifications. Recent research indicates that glycolysis-induced acetyl-CoA accumulation correlated with increased histone acetylation in microglia.[35] In pancreatic cancer cells, we observed elevated lactate and histone lactylation, with increased H3K18la promoting ACAT2 upregulation. This reinforces the notion that metabolic reprogramming may drive histone modification changes that impact gene expression. Given the co-variation of acetyl-CoA and lactate in glycolysis-dependent cells,[36] exploring histone lactylation and its impact on gene expression in pancreatic cancer is intriguing.

ACAT2 is critically involved in lipid metabolism by converting acetyl-CoA to acetoacetyl-CoA and CoA.[17 37] We discovered a novel role of ACAT2 in the acetylation and stabilisation of MTCH2, a critical protein for mitochondrial function.[19] MTCH2 loss has been reported to cause mitophagy dysregulation, mitochondrial fragmentation,[38] recruitment of tBID,[39] altered lipid homeostasis[40] and enhanced mitochondrial OXPHOS.[20] In MTCH2-deficient progenitors, lactate production decreases while mitochondrial respiration increases. Consistent with this, we found that increased ACAT2 expression hinders MTCH2 proteasomal degradation, leading to mitochondrial SRC downregulation and enhanced lactate production in pancreatic cancer cells, forming a positive feedback loop that increases H3K18la and ACAT2. This loop supports the notion that pancreatic cancer progression is an amplification process driven by an initial perturbation instead of a linear cascade.

ACAT2 is also critical for immune reprograming in pancreatic cancer. Inhibition of ACAT2 suppresses tumour growth and improves host survival by altering the immune landscape. We found that ACAT2 promotes M2-like polarisation of TAMs through cell–cell communication. Given that M2-like TAMs

suppress CD8$^+$ T cell cytotoxicity, our findings suggest targeting both ACAT2 and immune checkpoints may offer a promising therapeutic strategy. Our study highlights cholesterol as a key mediator in tumour cell-TAM communication. How does ACAT2 elevate the cholesterol secretion to TAMs? Cholesterol is well known to promote the production and release of sEVs and is enriched within them.[41] Given ACAT2's role in cholesterol synthesis,[37] it makes sense that it would contribute to sEV production and cholesterol release. The function of cholesterol in TME is still up for debate. Some studies suggest that cholesterol efflux disturbances promote M1 polarisation and enhance antitumour immunity.[42] Elevated cholesterol in the plasma membrane boosts CD8$^+$ T cell and NK cell function.[43 44] Conversely, cholesterol can also inhibit CD8$^+$ T cell activity by promoting immune checkpoint expression.[45] While cholesterol's role remains controversial, our research demonstrates that cholesterol promotes M2 macrophage polarisation, thereby suppressing antitumour immunity, highlighting its complex regulatory role in the TME.

This study highlights ACAT2's role in M2 polarisation and its impact on MTCH2 acetylation and stabilisation, driving an intracellular histone modification feedback loop that shapes the 'immune desert' in pancreatic cancer. In summary, our findings reveal the critical role of H3K18la/ACAT2/sEV-cholesterol signalling in tumour immunosuppressive reprogramming. As a heterobifunctional molecule, the PROTAC AP1 triggers ACAT2 *in vivo* degradation, offering lower toxicity and high selectivity compared with small molecule inhibitors. Therefore, targeted degradation of ACAT2 could reinforce antitumour immunity and synergistically amplify the response to anti-PD-1 therapy (figure 8).

Author affiliations
[1]Department of Pancreatic Surgery, Fudan University Shanghai Cancer Center, Shanghai, China
[2]Department of Oncology, Shanghai Medical College of Fudan University, Shanghai, China
[3]Shanghai Pancreatic Cancer Institute, Shanghai, China
[4]Shanghai Key Laboratory of Precision Medicine for Pancreatic Cancer, Shanghai, China
[5]Pancreatic Center Institute, Fudan University, Shanghai, China
[6]Department of General Surgery, First Affiliated Hospital of Dalian Medical University, Dalian, China
[7]Department of Hepatobiliary Pancreatic Surgery, The Affiliated Hospital of Qingdao University, Qingdao, China
[8]Key Laboratory of Growth Regulation and Translational Research of Zhejiang Province, School of Life Sciences, Westlake University, Hangzhou, China
[9]Tianjin Institute of Industrial Biotechnology, Chinese Academy of Sciences, Tianjin, China

Contributors JY performed most of the experiments and draft the manuscript. XiaoY and MX participated in the data analysis. HX, ZT, YL, YG, WW and JX provided technical support and research sources. SS and XianY designed the research. SS and XianY are responsible for the overall content as the guarantor. All the authors read and approved the final manuscript.

Funding This study was jointly supported by the National Natural Science Foundation of China (U21A20374and 92374102), Science and Technology Commission of Shanghai Municipality (YDZX20243100002003), Noncommunicable Chronic Diseases-National Science and Technology Major Project (2024ZD052550 0/2024ZD0525501/2024ZD0525505) and Natural Science Foundation of Shanghai (23ZR1479300).

Competing interests None declared.

Patient and public involvement Patients and/or the public were not involved in the design, or conduct, or reporting, or dissemination plans of this research.

Patient consent for publication Not applicable.

Ethics approval This study involves human participants and was approved by the Institutional Research Ethics Committee of FUSCC (Reference number: 2401290-12). Participants gave informed consent to participate in the study before taking part.

Provenance and peer review Not commissioned; externally peer reviewed.

Data availability statement All data relevant to the study are included in the article or uploaded as supplementary information.

Supplemental material This content has been supplied by the author(s). It has not been vetted by BMJ Publishing Group Limited (BMJ) and may not have been peer-reviewed. Any opinions or recommendations discussed are solely those of the author(s) and are not endorsed by BMJ. BMJ disclaims all liability and responsibility arising from any reliance placed on the content. Where the content includes any translated material, BMJ does not warrant the accuracy and reliability of the translations (including but not limited to local regulations, clinical guidelines, terminology, drug names and drug dosages), and is not responsible for any error and/or omissions arising from translation and adaptation or otherwise.

Open access This is an open access article distributed in accordance with the Creative Commons Attribution Non Commercial (CC BY-NC 4.0) license, which permits others to distribute, remix, adapt, build upon this work non-commercially, and license their derivative works on different terms, provided the original work is properly cited, appropriate credit is given, any changes made indicated, and the use is non-commercial. See: http://creativecommons.org/licenses/by-nc/4.0/.

ORCID iDs
Jing Yang http://orcid.org/0009-0003-2199-8623
Xiaoning Yu http://orcid.org/0009-0002-6288-4932
Mingming Xiao http://orcid.org/0000-0003-0862-2501
He Xu http://orcid.org/0000-0002-4044-3186
Zhen Tan http://orcid.org/0000-0002-6188-209X
Yubin Lei http://orcid.org/0000-0002-4468-8076
Yanmei Guo http://orcid.org/0000-0003-2610-9154
Wei Wang http://orcid.org/0000-0003-0286-6337
Jin Xu http://orcid.org/0000-0002-2942-8604
Si Shi http://orcid.org/0000-0002-6652-0629
Xianjun Yu http://orcid.org/0000-0002-6697-7143

REFERENCES

1 Siegel RL, Giaquinto AN, Jemal A. Cancer statistics, 2024. *CA Cancer J Clin* 2024;74:12–49.
2 Vincent A, Herman J, Schulick R, *et al*. Pancreatic cancer. *Lancet* 2011;378:607–20.
3 Conroy T, Hammel P, Hebbar M, *et al*. FOLFIRINOX or Gemcitabine as Adjuvant Therapy for Pancreatic Cancer. *N Engl J Med* 2018;379:2395–406.
4 Neoptolemos JP, Kleeff J, Michl P, *et al*. Therapeutic developments in pancreatic cancer: current and future perspectives. *Nat Rev Gastroenterol Hepatol* 2018;15:333–48.
5 Tempero MA. NCCN Guidelines Updates: Pancreatic Cancer. *J Natl Compr Canc Netw* 2019;17:603–5.
6 Morrison AH, Byrne KT, Vonderheide RH. Immunotherapy and Prevention of Pancreatic Cancer. *Trends Cancer* 2018;4:418–28.
7 Zhang Y, Zhang Z. The history and advances in cancer immunotherapy: understanding the characteristics of tumor-infiltrating immune cells and their therapeutic implications. *Cell Mol Immunol* 2020;17:807–21.
8 Sabari BR, Zhang D, Allis CD, *et al*. Metabolic regulation of gene expression through histone acylations. *Nat Rev Mol Cell Biol* 2017;18:90–101.
9 Zhang D, Tang Z, Huang H, *et al*. Metabolic regulation of gene expression by histone lactylation. *Nature New Biol* 2019;574:575–80.
10 Wang T, Ye Z, Li Z, *et al*. Lactate-induced protein lactylation: A bridge between epigenetics and metabolic reprogramming in cancer. *Cell Prolif* 2023;56:e13478.
11 Yu J, Chai P, Xie M, *et al*. Histone lactylation drives oncogenesis by facilitating m^{6}A reader protein YTHDF2 expression in ocular melanoma. *Genome Biol* 2021;22:85.
12 Pan R-Y, He L, Zhang J, *et al*. Positive feedback regulation of microglial glucose metabolism by histone H4 lysine 12 lactylation in Alzheimer's disease. *Cell Metab* 2022;34:634–48.
13 De Leo A, Ugolini A, Yu X, *et al*. Glucose-driven histone lactylation promotes the immunosuppressive activity of monocyte-derived macrophages in glioblastoma. *Immunity* 2024;57:1105–23.
14 Huang Z-W, Zhang X-N, Zhang L, *et al*. STAT5 promotes PD-L1 expression by facilitating histone lactylation to drive immunosuppression in acute myeloid leukemia. *Signal Transduct Target Ther* 2023;8:391.
15 Halbrook CJ, Lyssiotis CA, Pasca di Magliano M, *et al*. Pancreatic cancer: Advances and challenges. *Cell* 2023;186:1729–54.
16 Moreno-Yruela C, Zhang D, Wei W, *et al*. Class I histone deacetylases (HDAC1-3) are histone lysine delactylases. *Sci Adv* 2022;8:eabi6696.
17 Haapalainen AM, Meriläinen G, Wierenga RK. The thiolase superfamily: condensing enzymes with diverse reaction specificities. *Trends Biochem Sci* 2006;31:64–71.
18 Hornbeck PV, Zhang B, Murray B, *et al*. PhosphoSitePlus, 2014: mutations, PTMs and recalibrations. *Nucleic Acids Res* 2015;43:D512–20.
19 Guna A, Stevens TA, Inglis AJ, *et al*. MTCH2 is a mitochondrial outer membrane protein insertase. *Science* 2022;378:317–22.

20 Maryanovich M, Zaltsman Y, Ruggiero A, *et al*. An MTCH2 pathway repressing mitochondria metabolism regulates haematopoietic stem cell fate. *Nat Commun* 2015;6:7901.
21 Caronni N, La Terza F, Vittoria FM, *et al*. IL-1β+ macrophages fuel pathogenic inflammation in pancreatic cancer. *Nature New Biol* 2023;623:415–22.
22 Cassetta L, Pollard JW. Targeting macrophages: therapeutic approaches in cancer. *Nat Rev Drug Discov* 2018;17:887–904.
23 Ma S, Sun B, Duan S, *et al*. YTHDF2 orchestrates tumor-associated macrophage reprogramming and controls antitumor immunity through $CD8^+$ T cells. *Nat Immunol* 2023;24:255–66.
24 Ma X, Bi E, Lu Y, *et al*. Cholesterol Induces $CD8^+$ T Cell Exhaustion in the Tumor Microenvironment. *Cell Metab* 2019;30:143–56.
25 Yan C, Zheng L, Jiang S, *et al*. Exhaustion-associated cholesterol deficiency dampens the cytotoxic arm of antitumor immunity. *Cancer Cell* 2023;41:1276–93.
26 Ren L, Yi J, Li W, *et al*. Apolipoproteins and cancer. *Cancer Med* 2019;8:7032–43.
27 Möller A, Lobb RJ. The evolving translational potential of small extracellular vesicles in cancer. *Nat Rev Cancer* 2020;20:697–709.
28 Zhao S, Mi Y, Guan B, *et al*. Tumor-derived exosomal miR-934 induces macrophage M2 polarization to promote liver metastasis of colorectal cancer. *J Hematol Oncol* 2020;13:156.
29 Goswami S, Anandhan S, Raychaudhuri D, *et al*. Myeloid cell-targeted therapies for solid tumours. *Nat Rev Immunol* 2023;23:106–20.
30 Li J, Wu C, Hu H, *et al*. Remodeling of the immune and stromal cell compartment by PD-1 blockade in mismatch repair-deficient colorectal cancer. *Cancer Cell* 2023;41:1152–69.
31 Yi M, Zheng X, Niu M, *et al*. Combination strategies with PD-1/PD-L1 blockade: current advances and future directions. *Mol Cancer* 2022;21:28.
32 Irizarry-Caro RA, McDaniel MM, Overcast GR, *et al*. TLR signaling adapter BCAP regulates inflammatory to reparatory macrophage transition by promoting histone lactylation. *Proc Natl Acad Sci U S A* 2020;117:30628–38.
33 Li L, Chen K, Wang T, *et al*. Glis1 facilitates induction of pluripotency via an epigenome-metabolome-epigenome signalling cascade. *Nat Metab* 2020;2:882–92.
34 Thakur C, Chen F. Connections between metabolism and epigenetics in cancers. *Semin Cancer Biol* 2019;57:52–8.
35 Li Y, Lu B, Sheng L, *et al*. Hexokinase 2-dependent hyperglycolysis driving microglial activation contributes to ischemic brain injury. *J Neurochem* 2018;144:186–200.
36 Intlekofer AM, Finley LWS. Metabolic signatures of cancer cells and stem cells. *Nat Metab* 2019;1:177–88.
37 Song XQ, Fukao T, Yamaguchi S, *et al*. Molecular cloning and nucleotide sequence of complementary DNA for human hepatic cytosolic acetoacetyl-coenzyme A thiolase. *Biochem Biophys Res Commun* 1994;201:478–85.
38 Labbé K, Mookerjee S, Le Vasseur M, *et al*. The modified mitochondrial outer membrane carrier MTCH2 links mitochondrial fusion to lipogenesis. *J Cell Biol* 2021;220:e202103122.
39 Zaltsman Y, Shachnai L, Yivgi-Ohana N, *et al*. MTCH2/MIMP is a major facilitator of tBID recruitment to mitochondria. *Nat Cell Biol* 2010;12:553–62.
40 Rottiers V, Francisco A, Platov M, *et al*. MTCH2 is a conserved regulator of lipid homeostasis. *Obesity (Silver Spring)* 2017;25:616–25.
41 Pfrieger FW, Vitale N. Cholesterol and the journey of extracellular vesicles. *J Lipid Res* 2018;59:2255–61.
42 Sag D, Cekic C, Wu R, *et al*. The cholesterol transporter ABCG1 links cholesterol homeostasis and tumour immunity. *Nat Commun* 2015;6:6354.
43 Qin W-H, Yang Z-S, Li M, *et al*. High Serum Levels of Cholesterol Increase Antitumor Functions of Nature Killer Cells and Reduce Growth of Liver Tumors in Mice. *Gastroenterology* 2020;158:1713–27.
44 Yang W, Bai Y, Xiong Y, *et al*. Potentiating the antitumour response of CD8+ T cells by modulating cholesterol metabolism. *Nature New Biol* 2016;531:651–5.
45 Ma X, Bi E, Huang C, *et al*. Cholesterol negatively regulates IL-9-producing $CD8^+$ T cell differentiation and antitumor activity. *J Exp Med* 2018;215:1555–69.